

Global SLAM in Visual-Inertial Systems with 5G Time-of-Arrival Integration

Meisam Kabiri*, and Holger Voos*†

* *Interdisciplinary Center for Security Reliability and Trust (SnT)*

University of Luxembourg, Luxembourg

† *Faculty of Science, Technology, and Medicine (FSTM), Department of Engineering*

University of Luxembourg, Luxembourg

Email: {meisam.kabiri, holger.voos}@uni.lu

Abstract—This paper presents a novel approach to improve global localization and mapping in indoor drone navigation by integrating 5G Time of Arrival (ToA) measurements into ORB-SLAM3, a Simultaneous Localization and Mapping (SLAM) system. By incorporating ToA data from 5G base stations, we align the SLAM’s local reference frame with a global coordinate system, enabling accurate and consistent global localization. We extend ORB-SLAM3’s optimization pipeline to integrate ToA measurements alongside bias estimation, transforming the inherently local estimation into a globally consistent one. This integration effectively resolves scale ambiguity in monocular SLAM systems and enhances robustness, particularly in challenging scenarios where standard SLAM may fail. Our method is evaluated using five real-world indoor datasets collected with RGB-D cameras and inertial measurement units (IMUs), augmented with simulated 5G ToA measurements at 28 GHz and 78 GHz frequencies using MATLAB and QuaDRiGa. We tested four SLAM configurations: RGB-D, RGB-D-Inertial, Monocular, and Monocular-Inertial. The results demonstrate that while local estimation accuracy remains comparable due to the high precision of RGB-D-based ORB-SLAM3 compared to ToA measurements, the inclusion of ToA measurements facilitates robust global positioning. In scenarios where standard mono-inertial ORB-SLAM3 loses tracking, our approach maintains accurate localization throughout the trajectory.

Index Terms—5G Time of Arrival (ToA), Global Localization, Indoor Drone Navigation, ORB-SLAM3, Sensor Fusion, Visual-Inertial SLAM.

I. INTRODUCTION

Simultaneous Localization and Mapping (SLAM) systems are essential for autonomous robotics, enabling robots to construct maps of their environments while simultaneously determining their positions within those maps [1]. SLAM technologies are extensively utilized in fields such as autonomous navigation [2], augmented reality [3], and various robotic applications [4]. Most existing methods, primarily operate within a local reference frame, making it challenging

to achieve global localization, which is critical for large-scale environments, multi-agent systems, and integration with external infrastructure [5].

Integrating a global reference frame into SLAM systems addresses these challenges by anchoring localization to a consistent and absolute coordinate system. This enhancement improves positional accuracy, enables seamless interaction with external infrastructure, and supports collaborative multi-agent mapping [6], [7]. Additionally, a global reference frame allows SLAM systems to incorporate supplementary data sources, increasing reliability in scenarios where visual and inertial cues may be insufficient [8]. This integration also makes SLAM systems more scalable and adaptable for diverse real-world applications [9].

The advent of 5G technology has introduced advanced positioning capabilities, particularly through Time of Arrival (ToA) measurements [10], [11]. ToA provides highly accurate distance estimates between receivers and known base station positions, offering centimeter-level precision in ideal conditions. By incorporating ToA data, SLAM systems can align their local frames with a global reference frame defined by the fixed positions of 5G base stations. This global alignment enables robust localization and mapping in GPS-denied environments, enhancing applications like inventory management, real-time monitoring, autonomous vehicles, augmented reality, and emergency response. Drones, for instance, can autonomously navigate warehouses, accurately mapping the environment and tracking inventory levels, as illustrated in Figure 1. By leveraging ToA measurements from two 5G base stations as global anchors, drones achieve higher accuracy and robustness, optimizing inventory management and real-time monitoring processes.

This paper extends ORB-SLAM3 [12] by integrating 5G ToA measurements into its optimization pipeline to achieve globally consistent SLAM. Specifically, we introduce an SE3 transformation node into the estimation process, deeply integrating it into both the front-end and back-end modules of ORB-SLAM3. This SE3 node estimates the rigid body transformation between the local SLAM reference frame and the global 5G-based reference frame in real-time, aligning the local map with the global coordinate system to ensure precise localization and mapping across different environments.

This work was funded by the Luxembourg National Research Fund (FNR) 5G-SKY project (ref. C19/IS/13713801) and by the European Commission Horizon2020 research and innovation programme under the grant agreement No 101017258 (SESAME).

For the purpose of Open Access, and in fulfillment of the obligations arising from the grant agreement, the author has applied a Creative Commons Attribution 4.0 International (CC BY 4.0) license to any Author Accepted Manuscript version arising from this submission.



Fig. 1: Illustration of an indoor warehouse environment where a drone navigates while two 5G base stations provide Time-of-Arrival (ToA) measurements. The base stations assist in refining the drone’s positional accuracy, supporting real-time localization and mapping (The warehouse figure was generated using OpenAI’s ChatGPT).

Additionally, we incorporate bias nodes for each 5G base station to account for clock biases inherent in ToA measurements. These bias nodes are integrated into the optimization graph, allowing the system to jointly estimate the clock biases alongside the transformation between frames. This comprehensive integration of SE3 transformation and bias estimation ensures that the SLAM system maintains high performance and robustness, even in scenarios where traditional visual-inertial SLAM may encounter challenges such as feature-sparse environments or dynamic changes.

We assess the effectiveness of our approach using five indoor datasets captured with RGB-D cameras and Inertial Measurement Units (IMUs). These datasets are further enhanced with simulated 5G Time of Arrival (ToA) measurements at frequencies of 28 GHz and 78 GHz, generated using MATLAB and QuaDRiGa. The experimental results indicate that our method maintains high local estimation precision, benefiting from the accuracy inherent in RGB-D-based ORB-SLAM3. Moreover, the incorporation of ToA measurements significantly strengthens global localization and mapping reliability. Notably, in scenarios where the conventional mono-inertial ORB-SLAM3 fails to sustain tracking, our method consistently delivers accurate localization throughout the entire trajectory.

A. Contributions

The key contributions of this paper are as follows:

- **Integration of 5G ToA Measurements for Global SLAM:** We introduce a novel approach that integrates 5G Time of Arrival (ToA) measurements into the ORB-SLAM3 framework. This integration anchors the SLAM system’s local reference frame to a global coordinate

system defined by 5G base stations, enabling accurate and consistent global localization and mapping.

- **Resolving Scale Ambiguity in Monocular SLAM:** By incorporating ToA measurements, our method effectively resolves the scale ambiguity inherent in monocular SLAM systems. This allows for accurate metric scale estimation without the need for additional sensors or manual scaling.
- **Enhanced Robustness in Challenging Scenarios:** The deep integration of ToA measurements into ORB-SLAM3’s optimization pipeline enhances the system’s robustness, particularly in environments where standard SLAM may struggle, such as feature-sparse or dynamic settings. Our approach maintains accurate localization even when standard mono-inertial ORB-SLAM3 loses tracking.
- **Comprehensive Evaluation Using Real and Simulated Datasets:** We validate our approach using five real-world indoor datasets collected with RGB-D cameras and Inertial Measurement Units (IMUs), augmented with 5G ToA measurements simulated using MATLAB and QuaDRiGa. The evaluation demonstrates the effectiveness of our method in improving localization accuracy and robustness across various scenarios.

This paper is organized as follows. Section II reviews related work in visual SLAM, visual-inertial SLAM, and radio-based localization and SLAM. Section III details the methodology for integrating ToA measurements into ORB-SLAM3. Section IV describes the experimental setup and datasets used for evaluation. Section V presents and analyzes the results of the proposed method. Section VI discusses limitations and potential areas for future research, and Section VII concludes the paper with key findings and implications.

II. RELATED WORK

We review the literature under three categories: visual SLAM, visual-inertial SLAM, and radio-based SLAM, summarizing key advancements and challenges in each domain.

A. Visual Slam

Visual SLAM systems, which rely primarily on camera sensors, have undergone significant evolutionary stages in algorithmic development. Feature-based methods pioneered early advancements by extracting keypoints and descriptors from images to estimate camera motion and 3D structure. MonoSLAM [13] introduced real-time monocular SLAM using an Extended Kalman Filter (EKF) to track sparse feature points, laying groundwork for subsequent approaches. Parallel Tracking and Mapping (PTAM) [14] revolutionized the field by separating tracking and mapping into parallel threads, enabling more efficient Bundle Adjustment (BA) for improved pose estimation.

The ORB-SLAM series [15], [5], [12] marked a significant milestone by introducing robust feature extraction using Oriented FAST and Rotated BRIEF (ORB) descriptors [16]. These implementations progressively expanded SLAM

capabilities, with ORB-SLAM2 supporting monocular, stereo, and RGB-D cameras, and ORB-SLAM3 integrating visual-inertial capabilities and multi-map SLAM techniques.

Direct methods represent another critical approach, operating directly on pixel intensities without explicit feature extraction. Dense Tracking and Mapping (DTAM) [17] was among the first to use an inverse-depth representation for dense map construction. Large-Scale Direct SLAM (LSD-SLAM) [18] introduced a semi-dense approach focusing on high-gradient pixels, while Direct Sparse Odometry (DSO) [19] minimized photometric error over selected pixels.

Hybrid methods emerged to balance the strengths of feature-based and direct approaches. Semi-Direct Visual Odometry (SVO) [20] utilized direct methods for rotation estimation and feature-based methods for translation, achieving high-speed performance in dynamic environments. Direct Sparse Mapping (DSM) [21] further advanced this paradigm by introducing photometric Bundle Adjustment for global optimization.

Despite significant advancements, visual SLAM continues to face critical challenges: scale ambiguity in monocular systems, sensitivity to environmental conditions like lighting and texture variations, and the persistent need to balance computational complexity with real-time performance.

B. Visual-Inertial SLAM

Integrating Inertial Measurement Units (IMUs) with cameras addresses some limitations of visual SLAM by providing complementary motion information. IMUs offer high-frequency localization and orientation data, compensating for visual sensor shortcomings in fast motion or low-light conditions. Conversely, visual sensors help mitigate the cumulative drift commonly associated with IMUs, leading to more accurate and robust localization and mapping.

Filter-based approaches, such as Multi-State Constraint Kalman Filter (MSCKF) [22], MSCKF 2.0 [23], and Robust Visual-Inertial Odometry (ROVIO) [24], utilize recursive estimation techniques to fuse visual and inertial data. These methods primarily use Extended Kalman Filters (EKFs) to track system states and estimate uncertainties. MSCKF introduced a novel feature marginalization technique to decrease computational complexity, showing robustness during aggressive movements and brief feature losses. ROVIO extended this approach by incorporating direct photometric error minimization, particularly improving performance in low-texture environments. Optimization-based methods, including Open Keyframe-Based Visual-Inertial SLAM (OKVIS) [25], Visual-Inertial Navigation System (VINS-Mono) [26], VINS-Fusion [27], and ORB-SLAM3 [12], solve for system states by minimizing cost functions over data windows. These approaches employ advanced non-linear optimization techniques like bundle adjustment to ensure consistent mapping and localization throughout the trajectory. VINS implementations, for instance, utilized sliding window optimization frameworks that demonstrated remarkable robustness across diverse real-world datasets, while ORB-SLAM3 comprehensively integrated IMU data across multiple camera modalities.

Challenges in visual-inertial SLAM include accurate intrinsic and extrinsic calibration, robust initialization that involves scale and gravity estimation, handling dynamic environments, maintaining computational efficiency, and mitigating the effects of highly noisy IMU data.

C. Radio-Based Localization and SLAM

While visual and visual-inertial SLAM methods have shown remarkable performance, they often struggle in feature-sparse environments, under poor lighting conditions. These methods can also suffer from accumulated drift over time and the lack of absolute reference frames, particularly in GPS-denied or indoor environments.

Radio-based SLAM has emerged as a valuable complement to traditional methods. It leverages Radio Frequency (RF) signals—such as Ultra-Wideband (UWB), Wi-Fi, millimeter-wave (mmWave), and 5G technologies—for localization and mapping.

Recent advancements in localization techniques have explored innovative approaches for positioning mobile receivers in challenging environments [28]. Gentner et al. introduced Channel-SLAM, an algorithm leveraging multipath signals for positioning by treating multipath components as virtual transmitters and employing recursive Bayesian filtering with a Rao-Blackwellized particle filter. This approach demonstrates the potential of exploiting reflections and scattering without prior environmental knowledge, achieving accurate positioning in both line-of-sight and non-line-of-sight conditions. However, the method is computationally intensive and limited to multipath signal processing without incorporating visual or inertial sensors.

In a graph-based framework in radio SLAM, researchers have explored belief propagation and factor graphs to jointly localize mobile agents and map environments using multipath components [8], [29]. Specular reflections are modeled as virtual anchors (VAs), which are mirror images of physical anchors (PAs), allowing the system to simultaneously estimate the positions of VAs, PAs, and the mobile agent. Such techniques enhance localization accuracy by incorporating advanced signal parameters like the Angle of Arrival but often face challenges in computational complexity. Similarly, Chu et al. [30] and Mendrzik et al. [31] have investigated joint localization and radio mapping, using multipath information to estimate vehicle positions and environmental features simultaneously via factor graphs. However, their work neither utilized real data nor incorporated realistic network simulations and fusion schemes necessary for practical implementations.

Complementary approaches have utilized Wi-Fi technologies, such as 60 GHz IEEE 802.11ad, to provide indoor localization. Bielsa et al. [32] have developed a real-time system that achieves sub-meter accuracy in 70% of cases. While promising, these Wi-Fi-based methods may be limited by the quality of the wireless signal.

The emergence of 5G technology has further expanded localization possibilities for localization [9], [10]. Researchers developed frameworks like NR5G-SAM, presented in [9],

combined ToA and Received Signal Strength Indicator (RSSI) measurements with inertial sensing, employing factor graphs for trajectory estimation and Radio Environmental Map (REM) creation. This approach showed promise, especially in GNSS-denied and rural areas. However, it faced several limitations. The reliance on RSSI-based mapping reduced precision, particularly in vertical positioning. Additionally, the absence of loop closure mechanisms and dependence on multilateration increased computational demands. Del Peral-Rosado et al. [33] and Saleh et al. [34] explored 5G-based positioning techniques, achieving accuracies of 20-25 cm and sub-meter level, respectively. Other 5G-based localization methods have explored various techniques, including fingerprinting, machine learning, and signal processing. Talvitie et al. [35] utilized 5G synchronization signals to achieve sub-meter accuracy for high-speed train tracking. Zhang et al. [36] employed a deep neural network to improve positioning accuracy using 5G AoA and amplitude information, even in non-line-of-sight environments. Shamaei and Kassas [37] proposed an opportunistic ToA estimation approach using 5G synchronization signals and PBCH, achieving a ranging error standard deviation of 1.19 m. All of these studies primarily focused on localization and did not address the simultaneous mapping aspect of SLAM.

Recent research has also explored the integration of 5G Time-of-Arrival (ToA) measurements with inertial data for indoor localization. Kabiri et al. [38], [39] have investigated graph-based optimization and Error State Kalman Filter (ESKF)-based fusion approaches for Micro Aerial Vehicle (MAV) indoor localization. While these methods demonstrate promising results, they primarily focus on localization and do not explicitly address the simultaneous mapping aspect of SLAM.

Despite recent advancements in radio-based localization methods, particularly those leveraging 5G technologies, these approaches typically focus solely on localization without addressing the simultaneous mapping aspect essential for SLAM applications. Furthermore, most radio SLAM methods do not incorporate sensor fusion with visual data, relying instead on complex multipath signal processing alone. This lack of integration with additional sensor modalities limits their robustness and applicability in diverse and dynamic environments.

Our work distinguishes itself by integrating 5G ToA measurements into a state-of-the-art visual-inertial SLAM system, specifically extending ORB-SLAM3. By incorporating ToA data into the SLAM pipeline, we establish global localization within the reference frame defined by 5G base station placements.

To the best of our knowledge, this is the first study to combine 5G ToA measurements with visual-inertial SLAM for indoor drone navigation. Our approach addresses the limitations of prior methods by:

- **Simultaneous Localization and Mapping with Global Reference:** Unlike previous radio-based localization techniques that focus solely on positioning, our method simultaneously performs mapping while providing global

localization, enhancing the overall robustness and applicability of SLAM in indoor environments.

- **Integration without Compromising Local Accuracy:** We demonstrate that incorporating ToA measurements does not degrade the local estimation accuracy of ORB-SLAM3. This is crucial because it leverages the precision of visual-inertial SLAM while adding the benefits of global positioning.
- **Practical Implementation and Evaluation:** Our work includes the practical integration of 5G Time of Arrival (ToA) measurements into the SLAM system and extensive evaluation using real-world indoor datasets augmented with simulated ToA data. We generate 5G ToA measurements using QuaDRiGa and validate our approach across multiple real-world datasets, demonstrating its effectiveness in realistic scenarios.

III. METHODOLOGY

This section outlines the technical framework and processes to integrate ToA data into ORB-SLAM3 for globally consistent localization. We describe the distinction between local and global frames, ToA factor formulation, and the system modifications that enable robust pose estimation across diverse datasets.

A. Local Frame vs. Global Frame in SLAM

In SLAM, the concepts of local and global reference frames are fundamental for accurately representing and interpreting positional data within a mapped environment. A **local frame** is usually established at the beginning of the mission (e.g., at the first keyframe or the sensor's starting point). Once set, all subsequent poses, map points, and sensor measurements are calculated and expressed relative to this local coordinate system. While effective for maintaining local consistency, the local frame lacks alignment with a fixed real-world reference, leading to cumulative drift over time. Additionally, it can limit the system's ability to integrate or compare data from multiple sessions or external sources, which often require a global reference frame for alignment.

In contrast, a **global frame** is a fixed, absolute reference system tied to known landmarks or infrastructure, such as 5G base stations in our setup. This global frame provides a consistent anchor point independent of the SLAM system's starting pose. By aligning the local observations to the global frame, the SLAM system can mitigate drift, maintain long-term positional accuracy, and ensure interoperability with other systems or datasets operating in the same global context.

Figure 2 illustrates the distinction between the local and global frames and highlights the transformation process that bridges them. The local map, represented in red, depicts the environment relative to the initial sensor position. However, this map lacks global context, making it unsuitable for applications requiring absolute positioning. Conversely, the global map, depicted in teal, integrates ToA measurements from fixed base stations, which serve as global reference points. The

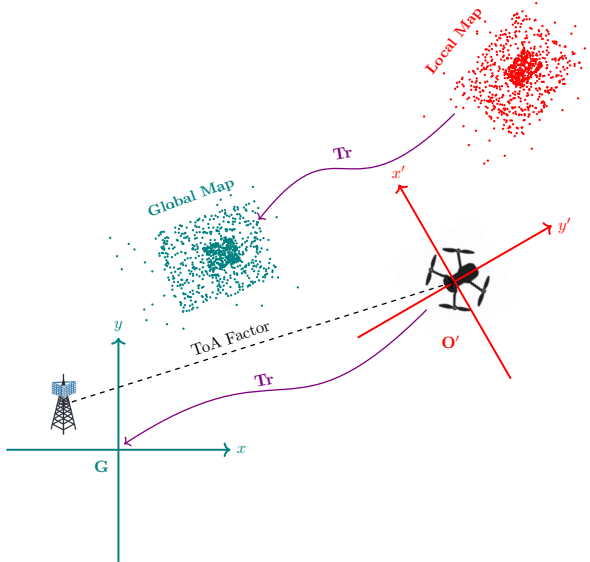


Fig. 2: Diagram depicting the relationship between the local and global maps in SLAM, highlighting the transformation \mathbf{Tr} that aligns local map coordinates (x', y') with the global coordinate frame (x, y) . The local map, represented in red, captures the same area as the global map in teal, with both maps displaying dense map points of equal scale. A base station, shown in the global frame, provides ToA measurements to refine positional accuracy. The dashed arrow from the global base station to the local frame indicates the impact of ToA measurements on the mapping process, linking local and global frames through \mathbf{Tr} .

transformation \mathbf{Tr} , shown in the figure, aligns the local frame to the global coordinate system, linking the two maps.

This alignment process is essential for achieving a globally consistent SLAM system. The transformation \mathbf{Tr} is estimated by leveraging ToA measurements, which provide spatial constraints based on the distances between the robot and the base stations. These constraints refine the local-to-global alignment and ensure that the trajectory and map points are accurately represented within the global frame. The dashed arrow in Figure 2 illustrates the influence of ToA measurements in bridging the local and global scales.

The integration of a global reference frame offers several advantages:

- **Drift Mitigation:** Periodic alignment with the global frame reduces cumulative drift inherent in local-only SLAM systems.
- **Multi-Agent Collaboration:** By operating within the same global frame, multiple robots or drones can share maps and coordinate actions effectively.
- **Robustness in Challenging Environments:** In scenarios with limited visual or inertial cues (e.g., featureless or dynamic environments), the global reference frame, established through methods such as 5G base stations or GPS, provides consistent positional information, ensuring

robustness and accuracy.

This distinction between local and global frames underpins the methodology used in this work, particularly in the integration of ToA data within ORB-SLAM3.

B. ToA Factor Formulation

ToA factor integrates distance measurements from base stations into the SLAM framework through a formulated error model. The factor connects multiple optimization vertices: the camera pose, local-to-global transformation, ToA measurement bias, and, in monocular cases, a scale factor. Figure 3 illustrates the structure of the ToA factor, highlighting how each component interacts within the optimization graph. The double-bordered base station nodes indicate that these parameters are fixed and their positions are known.

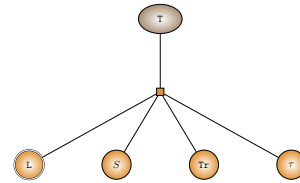


Fig. 3: Structure of the ToA factor, illustrating the key components: camera pose node (\mathbf{T}), scale factor (s), local-to-global transformation node (\mathbf{Tr}), base station position node (L), and bias node (τ). Double-bordered nodes indicate fixed parameters during optimization.

1) *Mathematical Formulation:* Let d_{meas} represent the measured distance affected by noise η^{Dist} and bias τ :

$$d_{\text{meas}} = d_{\text{true}} + \eta^{\text{Dist}} + \tau \quad (1)$$

The factor involves the following key components:

- Camera pose in the SLAM frame (local frame): \mathbf{T}_{oc}
- Local-to-global transformation: \mathbf{T}_{go}
- Base station position in global frame: L_G
- Scale factor (for monocular systems): s
- Bias of ToA distance measurement: τ

The transformation chain to calculate the keyframe pose in the global frame is given by:

$$\mathbf{T}_{gc} = \mathbf{T}_{go} \cdot \mathbf{T}_{oc} \quad (2)$$

The calculated distance between the camera and the base station is:

$$d_{\text{calculated}} = \|s \cdot t_{gc} - L_G\|_2 \quad (3)$$

where t_{gc} is the translation component of \mathbf{T}_{gc} , representing the camera's position in the global frame and s is the scaling parameter applied to account for scale differences, crucial in monocular SLAM systems where scale ambiguity exists. By introducing s into the error computation, the optimization can estimate the true metric scale of the environment:

- If s is known (e.g., in stereo or RGB-D systems), it can be fixed at $s = 1$.

- In monocular systems, s becomes an additional variable to estimate during optimization.

The ToA factor error is then computed as:

$$e = d_{\text{calculated}} - (d_{\text{meas}} - \tau) \quad (4)$$

The optimization framework minimizes a combined cost function for ToA measurements. For a single base station, the objective is to minimize the squared error between the measured and estimated TOAs:

$$\min_{\mathbf{T}_{oc}, \mathbf{T}_{go}, \tau, s} \sum_i (e_i)^2 \quad (5)$$

where i indexes the individual ToA measurement, and e_i is the error between the measured and estimated TOA for the i -th measurement. For multiple base stations, the objective function is extended to minimize the sum of squared errors across all base stations.

$$\min_{\mathbf{T}_{oc}, \mathbf{T}_{go}, \tau_j, s} \sum_i \sum_j (e_{i,j})^2 \quad (6)$$

where the summation spans all ToA measurements and their corresponding optimization variables.

- j indexes the base stations
- τ_j is the bias for the j -th base station
- $e_{i,j}$ is the error between the measured and estimated ToA for the i -th measurement at the j -th base station

2) *Uncertainty Propagation*: The information matrices (inverse covariance matrices) of both the scale parameter and the local-to-global transformation are suitably updated through the optimization process. These matrices are computed using the Hessian approximation derived from the Jacobians of the error terms with respect to the corresponding vertices. The updated uncertainties serve as prior information in subsequent optimization iterations, enabling a more robust convergence by:

- Providing appropriate weighting for new measurements based on accumulated certainty
- Preventing aggressive updates based on noisy or conflicting measurements to well-established estimates
- Allowing faster adaptation when uncertainty is high

C. System Components and Integration

1) *System Overview*: The proposed system integrates ToA measurements into the ORB-SLAM3 framework to achieve globally consistent localization and mapping. The main components of the system include tracking, local mapping, loop closing & ToA-based global map refinement. These components interact in a multi-threaded architecture to ensure real-time performance.

Figure 4 illustrates the system architecture, highlighting how ToA measurements are incorporated into the SLAM pipeline. Several existing components have been modified, including the Local Bundle Adjustment module, which now incorporates ToA measurements for improved optimization accuracy. The system diagram uses color coding to distinguish between

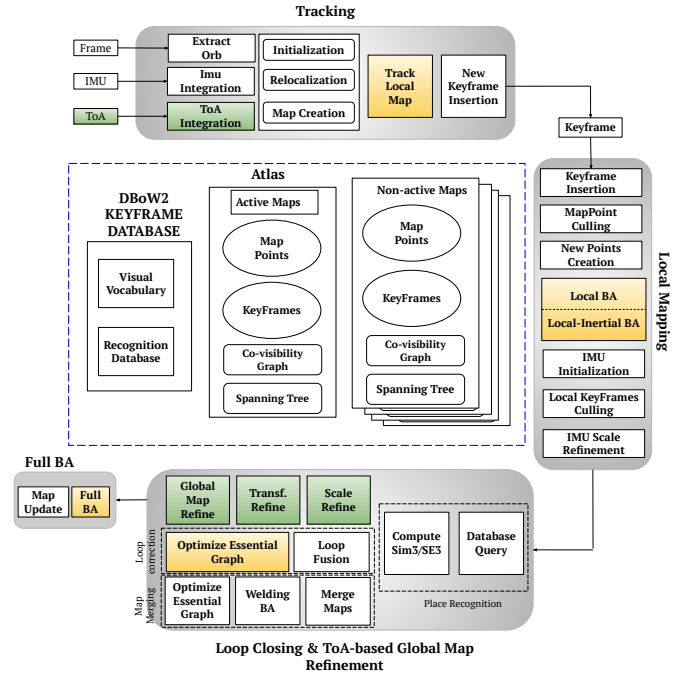


Fig. 4: Diagram of ORB-SLAM3 with ToA integration, illustrating the pipeline across Tracking, Local Mapping, and Loop Closing threads. New components are shown in green, including ToA-based global map refinement, while modified components are in yellow, such as Local Bundle Adjustment.

modifications to the original ORB-SLAM3 framework: new components are highlighted in green, while modified components are shown in yellow.

2) *System Integration*: The ToA measurements are integrated at multiple levels within the ORB-SLAM3 framework to maximize their utility while maintaining real-time performance, i.e., Tracking, Local Mapping, Loop Closing & ToA-based global map refinement. In what follows, we highlight some of the key changes and additions.

a) *Tracking Thread*: ToA factors are incorporated into frame-to-frame pose optimization, providing additional constraints during tracking. While this integration offers modest improvements, it can enhance robustness during rapid motion or feature-poor sequences. Fig. 5c illustrates the optimization structure in the Tracking thread, showing the interconnected nodes for the coming frame pose, map points, the local-to-global transformation, ToA biases, and base station positions (two are shown in the example). Two main factor types are integrated into the optimization process: ToA distance factors, as discussed earlier, and reprojection error factors. Reprojection error factors assess the difference between the observed location of a map point in an image and its projected position based on the estimated camera pose. By minimizing this error, we optimize the camera pose's alignment with the map.

b) *Local Mapping Thread*: Beyond the Tracking thread, ToA data is integrated into the Local Mapping thread to

refine keyframe poses, map points, and the local-to-global transformation. This is achieved through two optimization components:

- For systems without IMU data, the Local Bundle Adjustment incorporates visual features alongside the ToA measurements to optimize the poses of keyframes within the local optimization window, as well as the associated map points and the local-to-global transformation. This is illustrated in Fig. 5b, where the optimization graph includes nodes for keyframe poses, map points, and the transformation between the local and global coordinate frames.
- Local-Inertial Bundle Adjustment: For systems equipped with an IMU, the Local-Inertial Bundle Adjustment jointly considers visual, inertial, and ToA measurements in the optimization process. This combined optimization leads to more accurate pose and map estimation, especially in the presence of significant IMU noise. The structure of this optimization graph is shown in Fig. 5a, where the additional IMU-related factors are incorporated alongside the visual and ToA-based factors.

By leveraging ToA measurements in these Local Mapping optimizations, the ORB-SLAM3 system can further refine the estimates of keyframe poses, map points, and the local-to-global transformation, leading to improved overall accuracy and robustness. The inclusion of ToA data is particularly beneficial in scenarios where the visual information alone may be insufficient, such as in the presence of significant IMU noise or in feature-poor environments.

c) Loop Closing & ToA-based Global Map Refinement: One key component in Loop closing is the optimization of the Essential Graph which is responsible for Loop correction in which ToA edges are also added. The Essential Graph is a subset of the full map, containing all the keyframes and four types of edges:

- Odometry edges: These edges connect consecutive keyframes, representing the relative pose change between them.
- Covisibility edges: These edges connect keyframes that share a significant number of map points, representing the visual constraints between them.
- Loop closure edges: These edges are added when a loop closure is detected, providing additional constraints to correct drift and maintain global consistency.
- ToA-related edges

By incorporating ToA measurements into the Essential Graph optimization, we aim to improve the accuracy of keyframe poses by leveraging the additional spatial information from the ToA data and refine the local-to-global transformation.

d) New ToA-based Components: In addition to these modifications, there are also new components that are added, which we explain in the following section.

Global Map Refinement: A periodic global optimization process is performed to maintain the global consistency of the map using ToA. The optimization process is triggered by multiple conditions:

- Excessive ToA distance errors beyond measurement covariance thresholds
- Significant accumulated motion since last optimization
- Time-based triggers ensuring regular refinement
- Keyframe count thresholds

Figure 5d illustrates the optimization graph structure. It comprises keyframe pose nodes, transformation nodes, and bias nodes, interconnected by three types of edge types, Odometry edges (straight lines), Covisibility edges (angled lines connecting from above or below), and ToA-related edges.

This integrated approach combines odometry, visual, and ToA constraints to improve the accuracy of the estimated keyframe poses. After the keyframe poses are updated, the map points are also updated accordingly to maintain the consistency of the global map.

Transformation Refinement for Inertial Systems: In systems equipped with IMU, the initial estimation of the local-to-global transformation can be particularly challenging. When the initial guess for this transformation is far from the true value, the local inertial optimization in the Local Mapping thread can struggle to effectively leverage the ToA measurements to converge to the correct transformation. To mitigate this issue, we include a dedicated optimization process that focuses solely on refining the local-to-global transformation while keeping the keyframe poses fixed. This approach offers several advantages:

- Periodic Optimization of the local-to-global Transformation: The transformation refinement optimization is performed periodically within the Loop Closing & ToA-based Global Map Refinement thread, ensuring that the local-to-global transformation is regularly updated and maintained.
- Fixed Keyframe Poses: By keeping the keyframe poses fixed during this optimization, the system can ensure a stable convergence of the transformation estimates, without the additional complexity of jointly optimizing the poses and transformation.
- Enhanced Robustness against IMU Noise and Drift: The dedicated transformation refinement optimization, with fixed keyframe poses, is more robust against the effects of IMU noise and drift. This is particularly important in scenarios where the IMU measurements contain significant errors, as the optimization can focus solely on refining the transformation without being overly influenced by noisy inertial data.

The optimization graph for this transformation refinement process maintains a straightforward structure, incorporating only ToA and odometer edges. Figure 5e illustrates this graph structure.

Scale Refinement for Monocular Systems: Monocular visual SLAM systems inherently suffer from scale ambiguity. To address this, we incorporated a dedicated optimization component for global scale factor estimation and update.

This scale refinement is performed in addition to the local-to-global transformation while keeping keyframe poses fixed.

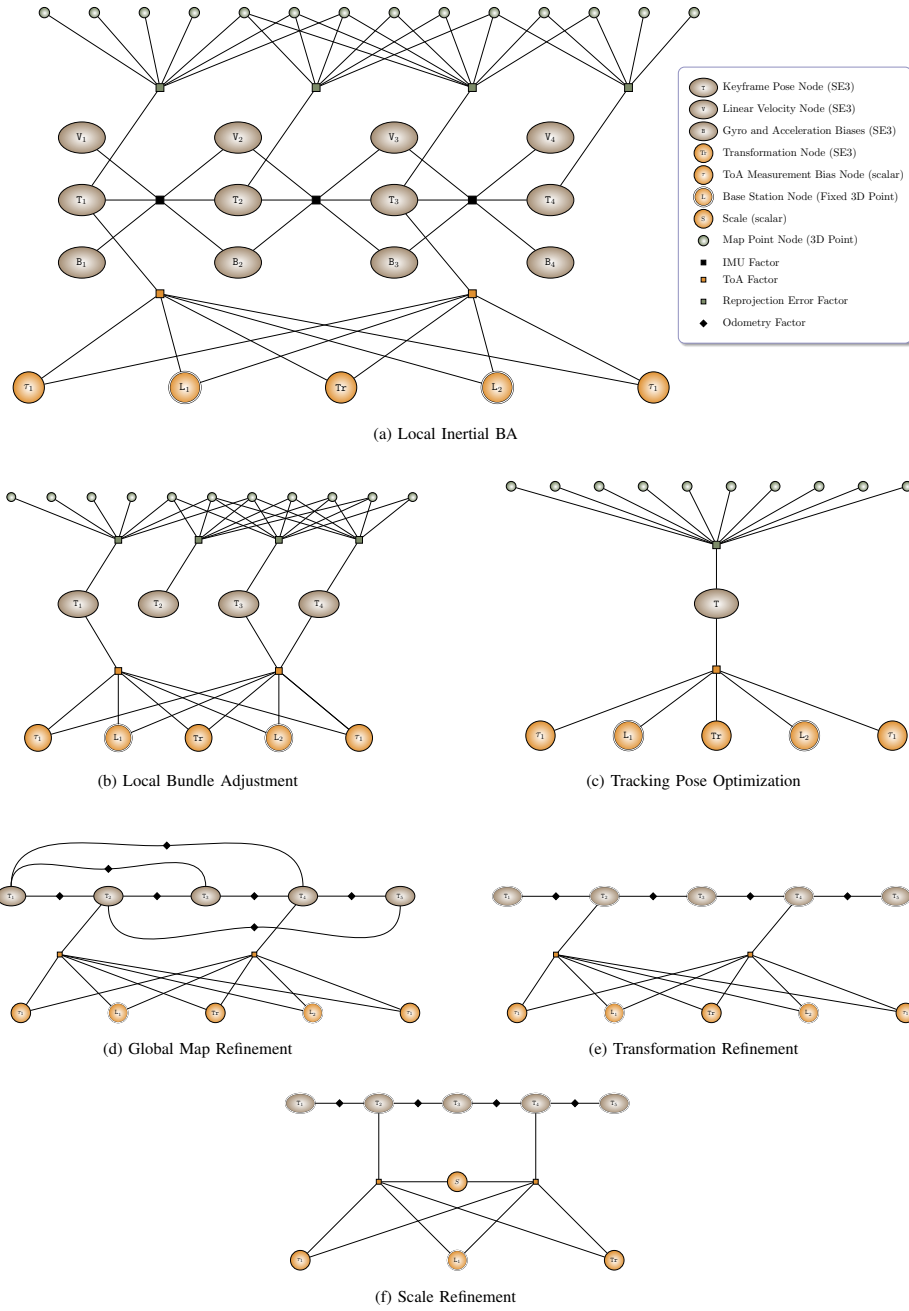


Fig. 5: Structures of optimization graphs for various components in the SLAM process: **(a) Local Inertial BA**: Optimization that integrates visual, inertial, and ToA measurements to refine keyframe poses and map points while addressing significant IMU noise. **(b) Local Bundle Adjustment**: Local refinement of keyframe poses, map points, ToA biases, and local-to-global transformations using visual and ToA constraints within a local optimization window. **(c) Tracking Pose Optimization**: Real-time optimization of the camera pose for the incoming frame by minimizing reprojection errors and incorporating ToA distance constraints. **(d) Global Map Refinement**: Global map refinement by leveraging odometry, co-visibility, loop closure, and ToA edges to improve global map consistency and keyframe accuracy. **(f) Transformation Refinement**: Periodic optimization focusing solely on refining the local-to-global transformation with fixed keyframe poses, enhancing robustness against IMU noise and drift. **(e) Scale Refinement**: A dedicated process for monocular SLAM systems to resolve scale ambiguity by optimizing the global scale factor, ensuring consistent keyframe poses and map points. **Note**: Double-bordered nodes in the graphs indicate fixed nodes during optimization.

By simplifying the graph to include only ToA edges, we enable global optimization, leveraging information from the entire keyframe map for a more accurate scale estimate. Figure 5f illustrates the structure of the scale refinement optimization graph. Key elements include: Keyframe pose nodes, scale factor node (s), ToA biases, and the Transformation node.

Optimizing the scale factor while keeping keyframe poses fixed efficiently estimates the correct global scale without introducing additional uncertainties or instabilities. The estimated scale factor is then propagated to update all keyframe poses and map point positions, ensuring a consistent and accurate global map representation.

The dedicated scale refinement optimization plays a crucial role in addressing the scale ambiguity inherent to monocular SLAM. While one might consider using the local mapping thread for this purpose, such an approach would be suboptimal for two key reasons. First, the optimization needs to handle significantly higher uncertainty levels, which can lead to instability when processed in local mapping. Second, updating both transformation and scale parameters through local mapping is inefficient, as it operates on a limited map section rather than leveraging the global map information available.

From an implementation standpoint, we utilized the existing three threads within ORB-SLAM3 without creating a new one. Specifically, we integrated the ToA-related global optimizations into the Loop Closing thread, which proved to be a natural and effective choice.

The integration of ToA measurements into the Loop Closing thread was selected for several reasons:

- 1) **Efficient Asynchronous Execution without Impacting Real-Time Tracking:** By incorporating the ToA-based optimizations into the asynchronous Loop Closing thread, we ensure that computationally intensive global optimizations are performed without affecting the real-time tracking performance in the Tracking thread. This approach efficiently utilizes system resources, preventing other threads from being burdened and maintaining overall system performance.
- 2) **Natural Integration with Global Map Maintenance and Separation of Concerns:** The Loop Closing thread is responsible for global map consistency tasks like loop closure detection and correction. Integrating the ToA-based optimizations into this thread allows us to seamlessly combine global map refinement processes, leveraging existing infrastructure and workflows. This also maintains a clear separation between local and global optimization tasks—the Tracking thread focuses on local pose optimization, and the Local Mapping thread handles local keyframe and map point refinement—ensuring that each thread operates effectively without interference.

IV. EXPERIMENT

This section presents a detailed evaluation of the proposed methodology. Our experiments are designed to assess the performance of the SLAM system under diverse configurations,

focusing on integrating simulated 5G ToA measurements with traditional visual and inertial data. The results provide insights into the impact of ToA integration across multiple datasets, sensor configurations, and 5G frequency bands.

A. Experimental Setup and Data Collection

The experiments were conducted in a controlled indoor environment, the Aerolab, specifically designed to support drone flights and data collection under realistic conditions for SLAM evaluation. The core equipment included an Intel RealSense D435i camera, used for RGB-D (color and depth) and IMU data acquisition, and the OptiTrack motion capture system, which provided high-precision ground truth data through a 12-camera configuration. Integrating these components enabled a comprehensive setup for acquiring synchronized data essential for SLAM.

The Intel RealSense D435i camera, mounted on the drone, captured RGB-D data at 30 Hz and IMU data at 200 Hz, with automatic synchronization between the visual and inertial data streams. To further support SLAM evaluation, five unique datasets were collected by flying the drone through varied trajectories that mimic realistic navigation scenarios, capturing a wide range of motion. Additionally, simulated 5G ToA data was generated at a rate of 10 Hz to complement the visual and inertial data. OptiTrack ground truth data was collected at 120 Hz, ensuring high accuracy and alignment with the other sensor modalities.

The drone operated within a netted 5x5x5 meter flight area for safety, though the Aerolab itself is larger, providing additional space for equipment and experimental setups. Each dataset represents a different flight path and duration, as detailed below:

- **Dataset 0:** 116 seconds
- **Dataset 1:** 110 seconds
- **Dataset 2:** 135 seconds
- **Dataset 3:** 124 seconds
- **Dataset 4:** 139 seconds

The trajectories for each dataset are visualized in Figure 6, where the top row displays the x-y trajectories and the bottom row illustrates the time vs. z plots.

The setup, including the drone equipped with the RealSense camera and the Aerolab environment, is illustrated in Figure 7. This figure provides visual context for the controlled flight space and the comprehensive equipment layout used for data collection.

The experiments were performed on a Ubuntu 20.04 laptop equipped with an Intel(R) Core(TM) i9-10885H CPU @ 2.40GHz with 16 cores and 32 GB of RAM.

To evaluate system robustness, we introduced significant noise to initial transformation estimates: 0.5m translation and 30° rotation for MONO mode, and 1m translation with 90° rotation for other modes. These substantial uncertainties effectively test the system’s trajectory recovery capabilities, simulating real-world scenarios where initial estimates may be imprecise.

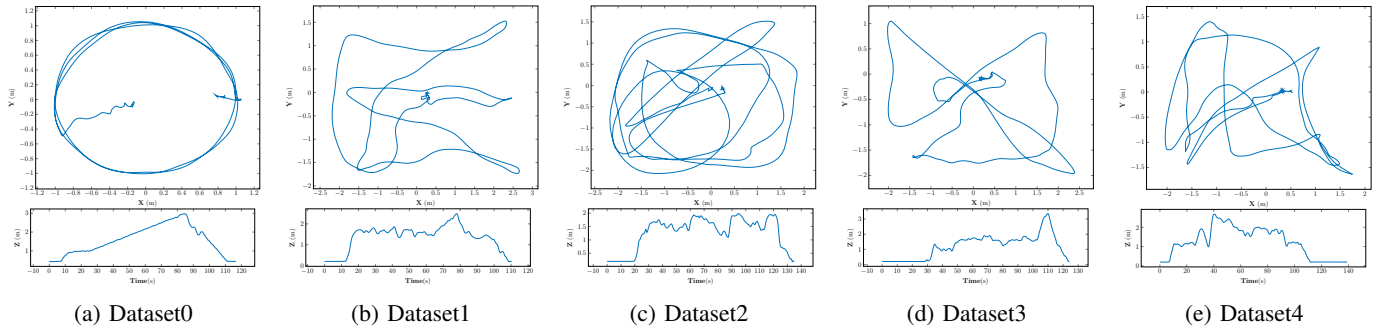


Fig. 6: Trajectories for the five Aerolab datasets. Each subfigure contains the x-y trajectory (top) and the time vs. z trajectory (bottom) for a specific dataset.

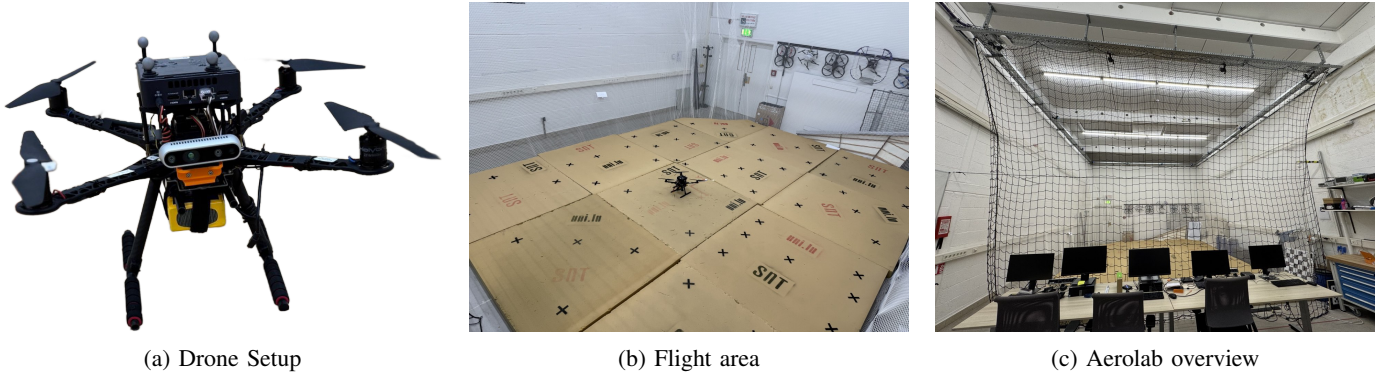


Fig. 7: (a) Drone equipped with an Intel RealSense D435i camera for RGB-D and IMU data acquisition. (b) Experimental flight area within the netted environment for safe indoor drone testing. (c) Overall view of the Aerolab, illustrating both the drone testing area and additional laboratory equipment and space.

B. Calibration and Data Synchronization

The intrinsic and extrinsic calibration of the camera and IMU was conducted using the `Kalibr` toolbox and `allan_variance_ros`. The calibration procedure involved collecting data with checkerboard patterns and performing specific drone motions. This process resulted in intrinsic parameters such as focal length and distortion coefficients, as well as the transformation matrix between the camera and IMU, crucial for accurate sensor fusion. Data synchronization is essential for optimal SLAM performance. Since the RealSense camera provides both RGB-D and IMU data, these streams are automatically synchronized. The OptiTrack system’s ground truth data is also time-aligned with the collected data. The 5G ToA measurements are simulated based on the OptiTrack trajectories, ensuring that all datasets are synchronized.

C. Augmenting the Dataset with Simulated 5G ToA Measurements

Acquiring real 5G ToA data in our lab setting is constrained by infrastructure and hardware limitations. To overcome this barrier, we employ a simulation-based approach to generate realistic ToA measurements. This strategy enables us to assess the advantages of integrating 5G positioning signals into the SLAM framework without the need for extensive physical

network setups. By combining simulated ToA data with authentic drone flight data—comprising RGB-D images, IMU readings, and precise ground truth trajectories—we construct an augmented dataset suitable for SLAM performance assessment. Figure 8 illustrates the overall structure of the simulation environment and how its components interact to generate this augmented dataset.

D. 5G ToA Simulation Methodology

Following our previous work [39], [38], we employ the same rigorous methodology to simulate 5G ToA measurements for the current dataset under the line-of-sight condition. The simulation framework utilizes the MATLAB 5G Toolbox to generate 5G signals, including Positioning Reference Signals (PRS) and Physical Downlink Shared Channel (PDSCH) resources, with consistent transmission parameters (0 dBm transmit power and 10 dB SNR).

The wireless channel characteristics are simulated using QuaDRiGa (quasi-deterministic radio channel generator) [40] with two distinct 5G FR2 (millimeter wave) network configurations: a 28 GHz configuration utilizing 200 MHz channel bandwidth with 120 kHz subcarrier spacing, and a 78 GHz configuration employing 400 MHz channel bandwidth with 240 kHz subcarrier spacing, both aligning with 3GPP specifications for FR2 deployments.

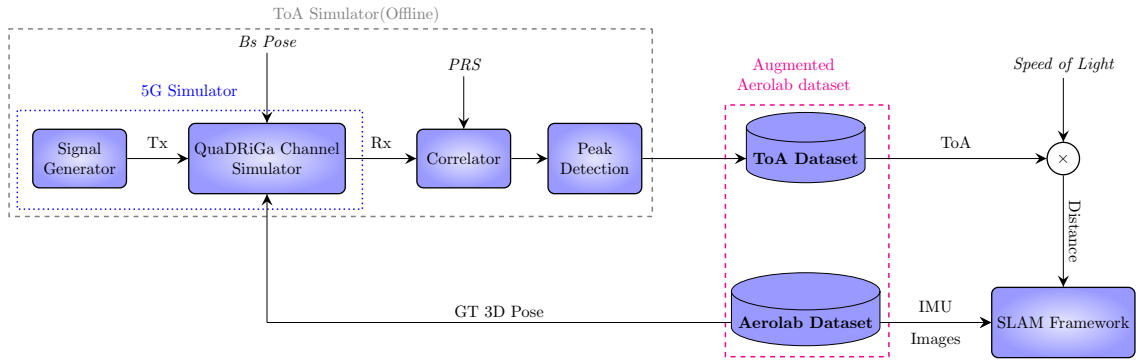


Fig. 8: Architecture of the dataset generation pipeline, showing the integration of simulated 5G ToA measurements with the Aerolab dataset. The pipeline consists of a 5G signal simulator using QuaDRiGa channel models, signal processing components (correlator and peak detection), and the final integration with IMU and image data from the Aerolab dataset. The combined data serves as input to the SLAM framework, with ToA measurements scaled by the speed of light to obtain distance measurements.

While the simulation framework remains unchanged, we adapt the base station placement to suit the current dataset’s environment. We virtually position four BSs within the experimental space, with coordinates defined in the OptiTrack system’s global frame as: BS1: (2.5, -2.5, 4.5), BS2: (2.5, 2.5, 4.0), BS3: (-2.5, 2.5, 5.0), BS4: (-6.5, -2.5, 2.0). The receiver is also assumed to be mounted on top of the drone.

The simulation maintains the established configuration parameters:

- Signal generation at 10 Hz (every 0.1 seconds)
- Empirically validated correlation threshold of 0.2 for ToA estimation
- Omnidirectional antenna configurations for both transmitters and receivers
- Consistent 5G system parameters across scenarios (bandwidth, subcarrier spacing, resource blocks, comb size, and cyclic prefix type)

The trajectory data from the current dataset is processed by computing velocities from consecutive pose measurements to maintain compatibility with the QuaDRiGa channel simulator’s requirements. This ensures that the simulated ToA measurements accurately reflect the dynamic characteristics of the platform’s motion in the new environment while maintaining consistency with our validated simulation methodology. The final statistics of the simulated ToA are given in Table I.

That table reveals differences between the two frequency bands across all datasets. The 78 GHz configuration demonstrates superior precision with standard deviations ranging from 14.25-19.58 cm, compared to the 28 GHz measurements which show larger variations of 27.64-41.32 cm. Mean errors at 78 GHz typically remain within ± 5 cm, while 28 GHz measurements exhibit larger systematic biases up to 19.41 cm. The 78 GHz configuration’s superior performance, evidenced by approximately 50% lower standard deviation and smaller systematic biases across all datasets, suggests it is the preferred choice for precise ToA measurements in indoor drone naviga-

tion scenarios. This performance advantage can be attributed to the larger bandwidth (400 MHz vs 200 MHz) and higher subcarrier spacing (240 kHz vs 120 kHz) available at 78 GHz.

E. Evaluation Metrics

We evaluated the system using the Absolute Trajectory Error (ATE) metric, comparing the estimated trajectories against the OptiTrack system’s ground truth. Two distinct evaluation approaches were employed:

- **Local Evaluation:** Before computing the ATE, we estimate and apply an optimal transformation (rotation, translation, and scale) between the SLAM-estimated trajectory and the ground truth. This alignment process factors out global positioning errors and evaluates the system’s ability to maintain consistent local trajectory shape and motion patterns. For example, if the drone flies in a square pattern, this evaluation would measure how well the SLAM system captures the square’s shape, regardless of its absolute position or orientation in space.
- **Global Evaluation:** No transformation or scale optimization was applied, enabling direct comparison between estimated and ground truth trajectories in their original coordinate frames. This approach provides a stringent assessment of the system’s ability to maintain accurate absolute positioning and orientation across the entire flight path.

Both evaluations were compared against the baseline ORB-SLAM3 system without ToA data integration, demonstrating how 5G measurements enhance global positioning capabilities while preserving local consistency.

V. RESULTS

In this section, we present and analyze the results of our experiments, which evaluate the performance of different SLAM modes integrated with 5G ToA data at two frequencies: 28 GHz and 78 GHz. The SLAM modes tested include RGB-D, RGB-D Inertial, Monocular (MONO), and Monocular

TABLE I: ToA Mean and Standard Deviation for 28 GHz and 78 GHz Frequencies Across Five Datasets and Four Base Stations

Dataset	Frequency (GHz)	Base Station	Std (cm)	Mean (cm)
Dataset0	28	1	32.92	4.20
		2	36.05	-1.21
		3	31.99	4.19
		4	41.32	8.28
	78	1	19.58	-2.71
		2	19.44	1.34
		3	19.10	0.31
		4	14.25	-1.72
Dataset1	28	1	36.31	-6.88
		2	29.60	-3.56
		3	36.60	1.88
		4	32.22	-2.68
	78	1	15.95	-2.83
		2	17.01	-2.29
		3	16.08	0.56
		4	15.64	-0.86
Dataset2	28	1	38.44	-8.24
		2	31.94	-4.93
		3	33.25	7.97
		4	30.49	-0.50
	78	1	15.83	0.87
		2	18.92	-4.97
		3	16.38	-0.80
		4	16.63	-0.59
Dataset3	28	1	40.14	-14.56
		2	32.19	-6.68
		3	31.17	4.49
		4	27.64	-4.97
	78	1	15.03	0.87
		2	17.61	-8.71
		3	14.69	-1.49
		4	15.94	-1.06
Dataset4	28	1	38.23	-19.41
		2	29.54	-2.18
		3	31.23	-3.09
		4	40.62	-8.31
	78	1	14.40	3.12
		2	16.80	-4.67
		3	15.56	0.57
		4	18.76	-1.08

Inertial. The performance is assessed on five datasets collected in the Aerolab environment, as described earlier.

For each experiment, we performed five runs to account for variability and ensure the robustness of the results. The values reported in Table II are the averages of the ATEs from these five runs. For enhanced clarity and visual representation, Fig.9 presents four bar charts illustrating the performance comparisons for the RGB-D, RGB-D Inertial, Monocular (MONO), and Monocular Inertial SLAM modes. These charts showcase the ATEs for both the baseline and the proposed ToA-integrated systems at 28 GHz and 78 GHz frequencies, with results evaluated under both local and global criteria across all datasets. The baseline global ATE values are omitted from the bar charts as they are significantly larger across all datasets, which would disproportionately scale the chart and reduce the visibility of the other results.

A. Evaluation Methodology: Local vs. Global Alignment

Before delving into the analysis, it is crucial to understand the difference between local and global evaluations and the

TABLE II: Average Errors for Different SLAM Modes

SLAM Mode	Dataset	Configuration	Local (m)	Global (m)
RGB-D	Dataset0	Baseline	0.064	2.857
		28 GHz ToA	0.066	0.237
		78 GHz ToA	0.055	0.101
	Dataset1	Baseline	0.116	2.739
		28 GHz ToA	0.117	0.165
		78 GHz ToA	0.117	0.133
	Dataset2	Baseline	0.155	2.930
		28 GHz ToA	0.160	0.197
		78 GHz ToA	0.148	0.158
	Dataset3	Baseline	0.095	2.594
		28 GHz ToA	0.102	0.149
		78 GHz ToA	0.094	0.104
Dataset4	Baseline	0.146	3.333	
	28 GHz ToA	0.162	0.242	
	78 GHz ToA	0.164	0.171	
RGB-D Inertial	Dataset0	Baseline	0.089	1.467
		28 GHz ToA	0.092	0.471
		78 GHz ToA	0.075	0.276
	Dataset1	Baseline	0.119	2.240
		28 GHz ToA	0.118	0.206
		78 GHz ToA	0.118	0.315
	Dataset2	Baseline	0.216	1.964
		28 GHz ToA	0.231	0.267
		78 GHz ToA	0.366	0.426
	Dataset3	Baseline	0.065	2.067
		28 GHz ToA	0.064	0.134
		78 GHz ToA	0.062	0.125
Dataset4	Baseline	0.108	1.947	
	28 GHz ToA	0.105	0.321	
	78 GHz ToA	0.105	0.168	
MONO	Dataset0	Baseline	-	-
		28 GHz ToA	-	-
		78 GHz ToA	-	-
	Dataset1	Baseline	1.370	2.458
		28 GHz ToA	0.059	0.380
		78 GHz ToA	0.058	0.121
	Dataset2	Baseline	1.284	2.323
		28 GHz ToA	0.089	0.186
		78 GHz ToA	0.075	0.152
	Dataset3	Baseline	1.363	2.404
		28 GHz ToA	0.058	0.162
		78 GHz ToA	0.058	0.127
Dataset4	Baseline	1.041	2.276	
	28 GHz ToA	0.179	0.320	
	78 GHz ToA	0.061	0.131	
MONO Inertial	Dataset0	Baseline	-	-
		28 GHz ToA	0.096	0.434
		78 GHz ToA	0.076	0.306
	Dataset1	Baseline	-	-
		28 GHz ToA	0.112	0.190
		78 GHz ToA	0.121	0.370
	Dataset2	Baseline	-	-
		28 GHz ToA	0.217	0.336
		78 GHz ToA	0.197	0.649
	Dataset3	Baseline	-	-
		28 GHz ToA	0.063	0.128
		78 GHz ToA	0.063	0.123
Dataset4	Baseline	-	-	
	28 GHz ToA	0.102	0.314	
	78 GHz ToA	0.102	0.150	

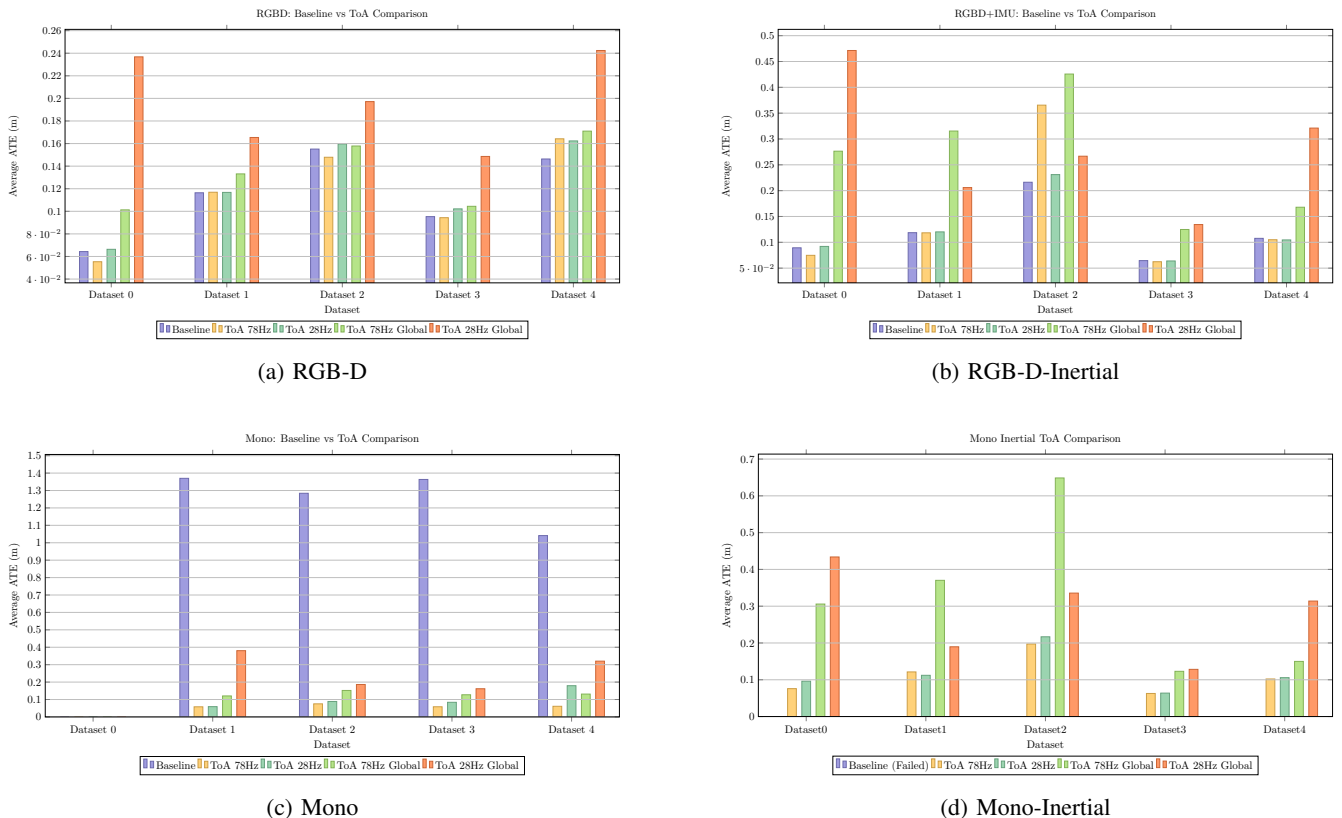


Fig. 9: Bar charts comparing Absolute Trajectory Errors (ATEs) for SLAM modes (a) RGB-D, (b) RGB-D-Inertial, (c) Mono, and (d) Mono-Inertial with and without ToA integration at 28 GHz and 78 GHz. Results are evaluated using local and global criteria across five datasets, with baseline global ATE values excluded for clarity..

implications of including baseline global results.

In the **local evaluation**, the transformation (rotation and translation) between the estimated trajectory and the ground truth is assumed to be unknown and is calculated offline after the SLAM process. This alignment is typically performed using methods like Horn’s absolute orientation algorithm, which finds the best-fit transformation that minimizes the trajectory error. Essentially, the local evaluation focuses on the consistency of the trajectory shape, disregarding the absolute positioning and orientation in the global frame.

In contrast, the **global evaluation** does not perform any post-processing alignment. The SLAM algorithm must estimate both the trajectory and the transformation directly, operating entirely in the global coordinate frame. This approach is more challenging because it requires the SLAM system to maintain accurate global positioning and orientation throughout the operation without relying on offline corrections. This challenge is highlighted in the 3D plots shown in Fig.10, which showcase one experiment (Dataset 0). Fig.10a shows the baseline RGB-D trajectory in its local frame, highlighting the misalignment with real-world coordinates. In contrast, Fig.10b presents the RGB-D trajectory enhanced with 78 GHz ToA measurements in the global frame, which closely matches the ground truth, demonstrating how ToA integration improves

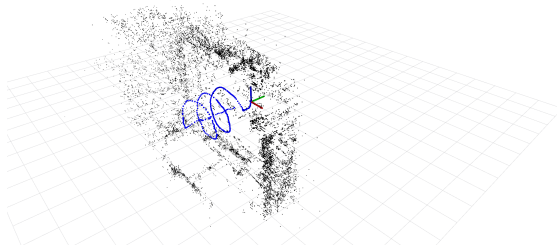
global consistency.

Including the **baseline global results** in our analysis provides insight into the ability of the baseline ORB-SLAM3 algorithm to estimate the global transformation without external aids like ToA data. However, it is important to note that the baseline algorithm is not designed to estimate global transformations during runtime in the absence of such data. Consequently, the baseline global errors are significantly higher than the local errors, as shown in Table II.

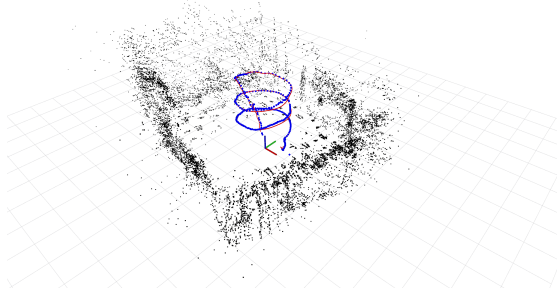
Comparing the baseline global results directly with the local results can be misleading or considered unfair because the baseline algorithm lacks the necessary information to perform global localization without external references. Therefore, when interpreting the results, one should consider the baseline global errors as a demonstration of the limitations of traditional SLAM algorithms in estimating absolute positions without additional data, rather than a direct performance comparison.

B. Analysis of SLAM Modes with ToA Integration

1) **RGB-D and RGB-D Inertial Modes:** For RGB-D SLAM mode, the baseline achieves exceptional local accuracy. Integrating 78 GHz ToA measurements shows slight improvements in most cases, while 28 GHz ToA integration results in minor degradation. This performance difference stems from two factors:



(a) Local estimate without alignment



(b) Global estimate with ToA at 78 GHz

Fig. 10: Comparison of RGB-D trajectory and map point estimates in local and global frames for Dataset 0. The SLAM results show keyframe pose estimates (blue lines), mapped features (black dots), and the ground truth trajectory (red line). Coordinate axes are color-coded: red for X, green for Y, and blue for Z. The local estimate (a) operates within the SLAM system’s frame, without real-world alignment. The global estimate (b), enhanced with 78 GHz ToA data, aligns closely with the ground truth in the global frame, demonstrating improved accuracy.

- **Baseline Superiority and 6-DoF Interpretation:** the baseline’s local accuracy already exceeds ToA measurement precision as shown in Table I. Additionally, ToA data offers only distance information, and translating these measurements into full 6-DoF pose estimations can inherently limit accuracy.
- **Post-Hoc Alignment and Fusion Complexity:** Post-hoc alignment compensates for global positioning errors, minimizing the impact of ToA integration on local accuracy. Furthermore, fusing additional sensor data introduces complexities and potential calibration challenges, which can lead to minor inconsistencies in the local ATEs.

For global evaluation, ToA integration significantly enhances performance, with 78 GHz measurements reducing global ATEs to approximately 0.1m across datasets, demonstrating effective global localization capabilities.

For the RGB-D Inertial mode, a similar trend is observed. ToA integration provides slight local improvements while significantly enhancing global localization performance, where

the baseline struggles without external references.

2) *Monocular (MONO) Modes:* For **MONO SLAM** mode, the baseline faces fundamental challenges from scale ambiguity and lack of depth information, resulting in high ATEs and complete failure on Dataset 0. Even with post-hoc alignment, local errors exceed 1m and global errors surpass 2m on other datasets.

ToA integration provides crucial scale and positioning information, significantly improving performance. At 78 GHz, global ATEs reduce to 0.121m on Dataset 1, compared to baseline errors exceeding 2m. Local performance also improves significantly, primarily due to better scale and transformation estimation during SLAM operations.

3) *Monocular Inertial Modes:* For **MONO Inertial** mode, the baseline fails across all datasets due to scale ambiguity and inertial sensor noise. ToA integration enhances both accuracy and robustness - enabling scale and global transformation estimation while stabilizing inertial data fusion. At 78 GHz, global ATEs reduce to 0.123m on Dataset 3.

However, challenges persist in some scenarios. Dataset 2’s global ATE remains high (0.649m) even with 78 GHz ToA data, indicating that while ToA integration helps overcome some limitations, managing multiple sensor modalities under varying conditions remains challenging.

C. Impact of 5G Network Frequency on ToA Performance

While the **78 GHz** 5G network configuration generally enables better ToA-based localization performance compared to **28 GHz** in the global evaluation, thanks to its greater bandwidth and subcarrier spacing, this pattern isn’t universal across datasets. Performance variations between the two configurations may arise from measurement noise and ToA estimation accuracy under different conditions.

In the local evaluation, differences between the two 5G network configurations are less pronounced due to the effects of post-hoc alignment. However, the improved precision of the 78 GHz configuration often results in better trajectory consistency in most scenarios.

D. Real-Time Performance

Our approach achieves real-time operation on ROS bag files at normal playback speed, running on a laptop with Intel i9-10885H CPU (2.40GHz, 16 cores) and 32GB RAM under Ubuntu 20.04. This computational efficiency makes the system practical for real-time drone navigation applications.

VI. SYSTEM LIMITATIONS AND FUTURE ENHANCEMENTS

While the experimental results demonstrate the efficacy of integrating simulated 5G ToA measurements with traditional visual and inertial data for SLAM, several limitations must be acknowledged:

- **Ideal Line-of-Sight (LoS) Conditions in ToA Simulation:** The current ToA simulation assumes ideal LoS conditions, which may not hold true in real-world scenarios. Non-Line-of-Sight (NLoS) conditions, caused by obstacles, can degrade ToA measurement accuracy and

impact SLAM performance. Future work needs more realistic channel models for complex environments.

- **Fixed Measurement Uncertainties:** The current approach uses static information matrices for ToA and visual-inertial measurements. Environmental factors can affect sensor reliability, requiring adaptive techniques that adjust measurement uncertainties dynamically.
- **Assumption of Fixed and Known Base Station Positions:** The experiments assume fixed and precisely known base station positions. In practical deployments, base stations may be mobile or have uncertain positions. Unknown or dynamically changing base station locations can significantly impact ToA-based localization. Future research should explore techniques for joint localization and base station position estimation to address this limitation.
- **Simulation-Based ToA Data Limitations:** Simulated ToA data may not fully capture real-world signal propagation complexities, hardware noise, and environmental dynamics. Validation with experimental ToA measurements is crucial for assessing practical performance.

VII. CONCLUSION

This paper presented a novel approach for integrating 5G ToA measurements with ORB-SLAM3 to enable globally consistent localization and mapping. Our method deeply embedded ToA data into the optimization framework, allowing real-time estimation of the transformation between local and global reference frames. Through extensive evaluation on five real-world datasets, we demonstrated that ToA integration maintained the high local accuracy of RGB-D SLAM while enabling robust global positioning. The approach proved particularly effective for monocular SLAM, resolving scale ambiguity and maintaining tracking where standard implementations failed. Future work should focus on addressing current limitations, including Non-Line-of-Sight conditions, adaptive measurement uncertainties, dynamic base station scenarios, and real-world ToA measurements. The successful integration of 5G ToA with visual-inertial SLAM opened new possibilities for robust indoor navigation, particularly in applications requiring precise global positioning like warehouse automation and drone navigation.

ACKNOWLEDGMENT

The authors would like to thank Hamed Habibi, Mohan Dasari, and Pedro Soares for their invaluable assistance with the experimental setup, flight operations, and data collection. Their support was pivotal to the success of this study.

REFERENCES

- [1] H. Durrant-Whyte and T. Bailey, "Simultaneous localization and mapping: part i," *IEEE robotics & automation magazine*, vol. 13, no. 2, pp. 99–110, 2006.
- [2] G. Grisetti, R. Kümmerle, C. Stachniss, and W. Burgard, "A tutorial on graph-based slam," *IEEE Intelligent Transportation Systems Magazine*, vol. 2, no. 4, pp. 31–43, 2010.
- [3] X. Sheng, S. Mao, Y. Yan, and X. Yang, "Review on slam algorithms for augmented reality," *Displays*, p. 102806, 2024.
- [4] G. Bresson, Z. Alsayed, L. Yu, and S. Glaser, "Simultaneous localization and mapping: A survey of current trends in autonomous driving," *IEEE Transactions on Intelligent Vehicles*, vol. 2, no. 3, pp. 194–220, 2017.
- [5] R. Mur-Artal and J. D. Tardós, "Orb-slam2: An open-source slam system for monocular, stereo, and rgb-d cameras," *IEEE transactions on robotics*, vol. 33, no. 5, pp. 1255–1262, 2017.
- [6] D. Zou, P. Tan, and W. Yu, "Collaborative visual slam for multiple agents: A brief survey," *Virtual Reality & Intelligent Hardware*, vol. 1, no. 5, pp. 461–482, 2019.
- [7] M. Karrer and M. Chli, "Towards globally consistent visual-inertial collaborative slam," in *2018 IEEE International Conference on Robotics and Automation (ICRA)*. IEEE, 2018, pp. 3685–3692.
- [8] E. Leitingner, F. Meyer, F. Tufvesson, and K. Witrisal, "Factor graph based simultaneous localization and mapping using multipath channel information," in *2017 IEEE International Conference on Communications Workshops (ICC Workshops)*. IEEE, 2017, pp. 652–658.
- [9] P. T. Karfakis, M. S. Couceiro, and D. Portugal, "Nr5g-sam: A slam framework for field robot applications based on 5g new radio," *Sensors*, vol. 23, no. 11, p. 5354, 2023.
- [10] R. M. Ferre, G. Seco-Granados, and E. S. Lohan, "Positioning reference signal design for positioning via 5g," *National Committee for Radiology in Finland*, 2019.
- [11] M. Kabiri, C. Cimarelli, H. Bavle, J. L. Sanchez-Lopez, and H. Voos, "A review of radio frequency based localisation for aerial and ground robots with 5g future perspectives," *Sensors*, vol. 23, no. 1, p. 188, 2022.
- [12] C. Campos, R. Elvira, J. J. G. Rodriguez, J. M. Montiel, and J. D. Tardós, "Orb-slam3: An accurate open-source library for visual, visual-inertial, and multimap slam," *IEEE Transactions on Robotics*, vol. 37, no. 6, pp. 1874–1890, 2021.
- [13] A. J. Davison, I. D. Reid, N. D. Molton, and O. Stasse, "Monoslam: Real-time single camera slam," *IEEE transactions on pattern analysis and machine intelligence*, vol. 29, no. 6, pp. 1052–1067, 2007.
- [14] G. Klein and D. Murray, "Parallel tracking and mapping for small ar workspaces," in *2007 6th IEEE and ACM international symposium on mixed and augmented reality*. IEEE, 2007, pp. 225–234.
- [15] R. Mur-Artal, J. M. M. Montiel, and J. D. Tardos, "Orb-slam: a versatile and accurate monocular slam system," *IEEE transactions on robotics*, vol. 31, no. 5, pp. 1147–1163, 2015.
- [16] E. Rublee, V. Rabaud, K. Konolige, and G. Bradski, "Orb: An efficient alternative to sift or surf," in *2011 International conference on computer vision*. Ieee, 2011, pp. 2564–2571.
- [17] R. A. Newcombe, S. J. Lovegrove, and A. J. Davison, "Dtam: Dense tracking and mapping in real-time," in *2011 international conference on computer vision*. IEEE, 2011, pp. 2320–2327.
- [18] J. Engel, T. Schöps, and D. Cremers, "Lsd-slam: Large-scale direct monocular slam," in *European conference on computer vision*. Springer, 2014, pp. 834–849.
- [19] J. Engel, V. Koltun, and D. Cremers, "Direct sparse odometry," *IEEE transactions on pattern analysis and machine intelligence*, vol. 40, no. 3, pp. 611–625, 2017.
- [20] C. Forster, Z. Zhang, M. Gassner, M. Werlberger, and D. Scaramuzza, "Svo: Semidirect visual odometry for monocular and multicamera systems," *IEEE Transactions on Robotics*, vol. 33, no. 2, pp. 249–265, 2016.
- [21] J. Zubizarreta, I. Aguinaga, and J. M. M. Montiel, "Direct sparse mapping," *IEEE Transactions on Robotics*, vol. 36, no. 4, pp. 1363–1370, 2020.
- [22] A. I. Mourikis and S. I. Roumeliotis, "A multi-state constraint kalman filter for vision-aided inertial navigation," *Proceedings of the IEEE International Conference on Robotics and Automation (ICRA)*, pp. 3565–3572, 2007.
- [23] C. Paul and S. I. Roumeliotis, "Mscf 2.0: Multi-state constraint kalman filter with observability-based consistent ekf for robust visual-inertial navigation," *Proceedings of the IEEE International Conference on Robotics and Automation (ICRA)*, pp. 2421–2428, 2017.
- [24] M. Bloesch, M. Burri, H. Sommer, R. Siegwart, and A. Nüchter, "Robust visual inertial odometry using a direct ekf-based approach," *Proceedings of the IEEE/RSJ International Conference on Intelligent Robots and Systems (IROS)*, pp. 298–304, 2015.
- [25] S. Leutenegger, S. Lynen, M. Bosse, R. Siegwart, and P. Furgale, "Keyframe-based visual-inertial odometry using nonlinear optimization," *The International Journal of Robotics Research*, vol. 34, no. 3, pp. 314–334, 2015.

- [26] T. Qin, P. Li, and S. Shen, "Vins-mono: A robust and versatile monocular visual-inertial state estimator," *IEEE transactions on robotics*, vol. 34, no. 4, pp. 1004–1020, 2018.
- [27] T. Qin, S. Cao, J. Pan, and S. Shen, "A general optimization-based framework for global pose estimation with multiple sensors," *arXiv preprint arXiv:1901.03642*, 2019.
- [28] C. Gentner, T. Jost, W. Wang, S. Zhang, A. Dammann, and U.-C. Fiebig, "Multipath assisted positioning with simultaneous localization and mapping," *IEEE Transactions on Wireless Communications*, vol. 15, no. 9, pp. 6104–6117, 2016.
- [29] E. Leitinger, F. Meyer, F. Hlawatsch, K. Witrissal, F. Tufvesson, and M. Z. Win, "A belief propagation algorithm for multipath-based slam," *IEEE transactions on wireless communications*, vol. 18, no. 12, pp. 5613–5629, 2019.
- [30] X. Chu, Z. Lu, D. Gesbert, L. Wang, and X. Wen, "Vehicle localization via cooperative channel mapping," *IEEE Transactions on Vehicular Technology*, vol. 70, no. 6, pp. 5719–5733, 2021.
- [31] R. Mendrzik, H. Wymeersch, and G. Bauch, "Joint localization and mapping through millimeter wave mimo in 5g systems," in *2018 IEEE Global Communications Conference (GLOBECOM)*. IEEE, 2018, pp. 1–6.
- [32] G. Bielsa, J. Palacios, A. Loch, D. Steinmetzer, P. Casari, and J. Widmer, "Indoor localization using commercial off-the-shelf 60 ghz access points," in *IEEE INFOCOM 2018-IEEE Conference on Computer Communications*. IEEE, 2018, pp. 2384–2392.
- [33] J. A. del Peral-Rosado, J. A. López-Salcedo, S. Kim, and G. Seco-Granados, "Feasibility study of 5g-based localization for assisted driving," in *2016 International conference on localization and GNSS (ICL-GNSS)*. IEEE, 2016, pp. 1–6.
- [34] S. Saleh, A. S. El-Wakeel, and A. Noureldin, "5g-enabled vehicle positioning using ekf with dynamic covariance matrix tuning," *IEEE Canadian Journal of Electrical and Computer Engineering*, vol. 45, no. 3, pp. 192–198, 2022.
- [35] J. Talvitie, T. Levanen, M. Koivisto, K. Pajukoski, M. Renfors, and M. Valkama, "Positioning of high-speed trains using 5g new radio synchronization signals," in *2018 IEEE Wireless Communications and Networking Conference (WCNC)*. IEEE, 2018, pp. 1–6.
- [36] Z. Zhang, L. Wu, Z. Zhang, J. Dang, B. Zhu, and L. Wang, "Aoa-and-amplitude fingerprint based indoor intelligent localization scheme for 5g wireless communications," in *2021 13th International Conference on Wireless Communications and Signal Processing (WCSP)*. IEEE, 2021, pp. 1–5.
- [37] K. Shamaei and Z. M. Kassas, "Receiver design and time of arrival estimation for opportunistic localization with 5g signals," *IEEE Transactions on Wireless Communications*, vol. 20, no. 7, pp. 4716–4731, 2021.
- [38] M. Kabiri, C. Cimorelli, H. Bavle, J. L. Sanchez-Lopez, and H. Voos, "Pose graph optimization for a mav indoor localization fusing 5gnr toa with an imu," in *2023 13th International Conference on Indoor Positioning and Indoor Navigation (IPIN)*. IEEE, 2023, pp. 1–6.
- [39] —, "Graph-based vs. error state kalman filter-based fusion of 5g and inertial data for mav indoor pose estimation," *Journal of Intelligent & Robotic Systems*, vol. 110, no. 2, p. 87, 2024.
- [40] S. Jaeckel, L. Raschkowski, K. Börner, L. Thiele, F. Burkhardt, and E. Eberlein, "Quadriga-quasi deterministic radio channel generator, user manual and documentation," *Fraunhofer Heinrich Hertz Institute, Tech. Rep. v2. 0.0*, 2017.